Hindawi Publishing Corporation
Journal of Nanomaterials
Volume 2012, Article ID 929278, 7 pages
doi:10.1155/2012/929278

Research Article

Crystallinity Improvement of ZnO Thin Film on Different Buffer Layers Grown by MBE

Shao-Ying Ting,[1] Po-Ju Chen,[2,3] Hsiang-Chen Wang,[2,3] Che-Hao Liao,[1] Wen-Ming Chang,[1] Ya-Ping Hsieh,[2,3] and C. C. Yang[1]

[1] *Institute of Photonics and Optoelectronics, National Taiwan University, Taipei 10617, Taiwan*
[2] *Graduate Institute of Opto-Mechatronics, National Chung Cheng University, Chia-Yi 62102, Taiwan*
[3] *Advanced Institute for Manufacturing with High-Tech Innovations, National Chung Cheng University, Chia-Yi 62102, Taiwan*

Correspondence should be addressed to Hsiang-Chen Wang, hcwang@ccu.edu.tw

Received 23 November 2011; Revised 1 February 2012; Accepted 2 February 2012

Academic Editor: J. C. Sczancoski

The material and optical properties of ZnO thin film samples grown on different buffer layers on sapphire substrates through a two-step temperature variation growth by molecular beam epitaxy were investigated. The thin buffer layer between the ZnO layer and the sapphire substrate decreased the lattice mismatch to achieve higher quality ZnO thin film growth. A GaN buffer layer slightly increased the quality of the ZnO thin film, but the threading dislocations still stretched along the *c*-axis of the GaN layer. The use of MgO as the buffer layer decreased the surface roughness of the ZnO thin film by 58.8% due to the suppression of surface cracks through strain transfer of the sample. From deep level emission and rocking curve measurements it was found that the threading dislocations play a more important role than oxygen vacancies for high-quality ZnO thin film growth.

1. Introduction

Recently, ZnO has received considerable attention due to its excellent emission properties in the UV region. ZnO is a direct band-gap material with wurtzite-structure, exhibits a wide band-gap of 3.37 eV, and has a large exciton binding energy of 60 meV at room temperature [1]. Based on these fundamental properties, ZnO has many applications in the short wavelength region such as optically pumped lasers, UV light emitting diodes, detectors, solar cells, and gas sensors [2–6]. However, the growth of ZnO thin film for such applications still remains problematic. So far, various methods have been employed to grow high quality ZnO thin films, for example, sputtering, pulsed laser deposition, metal organic chemical vapor deposition (MOCVD), and molecular beam epitaxy (MBE) [7–10]. MBE is a promising technique for the growth of high quality ZnO thin films due to its operation in ultra-high-vacuum conditions ($> 10^{-9}$ torr), using ultra pure substrates (6 N), and Angstrom-scale-thickness control. ZnO films are grown on different substrates including c-Al_2O_3, ZnO, GaN, and $ScAlMgO_4$. Among these substrates, c-Al_2O_3 is the most frequently used because of its low price, ease of producing large wafers, and ready availability for growing epitaxial films [11]. When ZnO films are grown on c-Al_2O_3 substrates without a buffer layer, however, the ZnO films generally show poor crystalline quality with a high dislocation density because of the 18% lattice mismatch between ZnO and c-Al_2O_3. Furthermore, a large difference in the thermal expansion coefficients between ZnO and c-Al_2O_3 ($\alpha_{ZnO} = 6.51 \times 10^{-6}\,K^{-1}$ and $\alpha_{sapphire} = 8.00 \times 10^{-6}\,K^{-1}$) will generate strain under the high temperature growth conditions. Chen et al. demonstrated a two-step growth method that carries out the initial growth at a lower temperature followed by a growth step at high temperature. Through this method a densely packed ZnO film with larger grains and well-aligned crystallographic orientation can be obtained [12].

In addition, the improvement in growth quality by using a buffer layer to decrease the lattice mismatch between ZnO and c-Al_2O_3 is a well-known method. These thin buffer layers for growing ZnO are GaN, MgO, ZnS, or SiC [13–16]. GaN and MgO are the most popular buffer layers for

ZnO grown on sapphire substrate. With the GaN buffer layer, the similar lattice structure, low lattice mismatch between ZnO and GaN, and similar thermal expansion coefficients ($\alpha_{GaN} = 5.59 \times 10^{-6}\,K^{-1}$) provide suitable conditions for ZnO growth [17]. Thus, a GaN buffer layer can solve the cracking problem during the quick growth of ZnO thin films by acting as a homoepitaxy quasi substrate [18]. A ZnO thin film on a GaN buffer layer on a c-sapphire substrate does, however, suffer compressive stress.

When using MgO as a buffer layer there are two approaches to solving the issues of high quality ZnO growth. For high temperature growths (750–850°C), the interaction between MgO and Al_2O_3 dominats: the Mg^{2+} and Al^{3+} diffuse to form a spinel intermediate layer ($MgAl_2O_4$). The 18% lattice mismatch between ZnO and Al_2O_3 is stepwise divided between ZnO/MgO, MgO/spinel, and spinel/Al_2O_3. A maximum mismatch of about 9.2% remains at the ZnO/MgO interface while the lattice mismatch between the MgO grains and the spinel layer is about 5.6%. Experiments reveal that the density of threading dislocation decreases by a factor of five when using MgO as the buffer layer [19].

For ZnO growth at low temperature (~600°C), the reaction between MgO and Al_2O_3 cannot occur, but the MgO buffer layer still decreases the lattice mismatch during the ZnO growth. For thin MgO layers, the ZnO grown on the MgO layer is a layer-by-layer epitaxy and the threading dislocations cannot stretch along the *c*-axis of the ZnO. In such a condition, the threading dislocations of the ZnO cluster occur only within 20 nm of the ZnO/MgO interface, which can improve the crystallization quality of the ZnO growth [20, 21].

In this paper, the growth of ZnO thin films on *c*-plane sapphire substrates by a two-step temperature variation was demonstrated using different MBE-deposited buffer layers. Temperature-dependent photoluminescence results showed the optical features of ZnO thin film samples with and without buffer layers. The crystallization quality and strain distribution of ZnO structures were analyzed through X-ray diffraction (XRD) and X-ray rocking curve (XRC) measurements. The surface morphologies of the ZnO thin films were studied by atomic force microscopy (AFM) and scanning electron microscopy (SEM). The ZnO thin film with a 7 nm thick MgO buffer layer, 18 nm thick low-temperature-grown ZnO layer, and 100 nm thick high-temperature-grown ZnO layer showed the best crystallization properties in this study.

2. Growth Conditions and Structures of the Growth Samples

The ZnO thin films were grown on commercial (0001) c-Al_2O_3 substrates by MBE. For Sample A, ZnO was grown with a thickness of 6 nm at low temperature (LT) on the c-Al_2O_3 substrate with no buffer layer. In this step, the growth temperature, beam equivalent pressure, and O_2 flow rate were 500°C, 5×10^{-7} torr, and 3 sccm, respectively. Then ZnO was grown with a thickness of 600 nm at high temperature (HT) on the LT-ZnO layer. In this step, the growth temperature, beam equivalent pressure, and O_2 flow rate were 600°C, 6×10^{-7} torr, and 4 sccm, respectively. Sample B is a ZnO thin film on a GaN buffer layer. The GaN buffer layer was grown on a c-Al_2O_3 substrate at 1,000°C with a thickness of 2 μm by MOCVD. Then the LT-ZnO was grown with a thickness of 10 nm on the GaN buffer layer. In this step, the growth temperature, beam equivalent pressure, and O_2 flow rate were 300°C, 5×10^{-7} torr, and 3 sccm, respectively. Finally, HT-ZnO was grown with a thickness of 250 nm on the LT-ZnO layer. In this step, the growth temperature, beam equivalent pressure, and O_2 flow rate were 600°C, 5×10^{-7} torr, and 2 sccm, respectively. Samples C, D, and E were ZnO thin films on 7 nm thick MgO buffer layers, which were grown on c-Al_2O_3 substrates. In this step, the growth temperature, beam equivalent pressure, and O_2 flow rate were 550°C, 2×10^{-7} torr, and 3 sccm, respectively. For these samples, the growth conditions of the LT-ZnO layers were the same as for Sample B. But sample D had an 18 nm-thick LT-ZnO layer. For the HT-ZnO layers, these three samples had the same growth temperature of 600°C as for Sample B. In this step, the growth thickness, beam equivalent pressure, and O_2 flow rate of Samples C, D, and E were 400 nm, 7.5×10^{-7} torr, and 3.5 sccm; 100 nm, 5.0×10^{-7} torr, and 2.5 sccm; 100 nm, 5.0×10^{-7} torr, and 1.4 sccm, respectively. Figure 1 summarizes the layer structures of the samples.

Samples A, B, C, and D were grown in an O_2-rich condition. Sample E was grown in the stoichiometric condition ($Zn : O_2 = 1 : 1$), which results in more oxygen vacancies. After the HT-ZnO layers' growth, all of the samples were annealed at 700°C for 10 minutes to improve crystallization. Table 1 shows the growth parameters of the samples.

3. XRD and XRCs Measurements

Figure 2 shows the XRD spectra of the samples with only (002) ZnO peak. Figure 3 shows the normalized XRC results of the samples. In this figure, the largest full width at half maximum (FWHM) of 791.74 arcsec was measured in Sample A, which indicated that a high density of threading dislocations existed due to a larger lattice mismatch between ZnO and c-Al_2O_3. The FWHM of Sample B was 242.58 arcsec, a 69.40% decrease from sample A. This decrease came from the small lattice mismatch of 1.80% between ZnO and GaN, which resulted in a decrease of the dislocation density in the ZnO layer. However, many threading dislocations still existed in the GaN buffer layer due to the larger lattice mismatch of 16% between GaN and the c-Al_2O_3 substrate. In this study, the GaN buffer layer in Sample B was thicker than MgO buffer layers in Samples C, D, and E to minimize the influence of lattice mismatch between GaN and c-Al_2O_3 for high quality ZnO thin film growth [13]. Thus, the GaN buffer layer showed some limitations for high quality ZnO thin film growth. The FWHM of Samples C, D, and E are 64.18, 48.66, and 98.01 arcsec, respectively, representing 91.89%, 93.85%, and 87.60% decreases compared to Sample A. These results indicate the higher quality of ZnO growth on an MgO buffer layer. Although the lattice mismatch between MgO and ZnO of 8.4% is more than that between ZnO and GaN (1.8%),

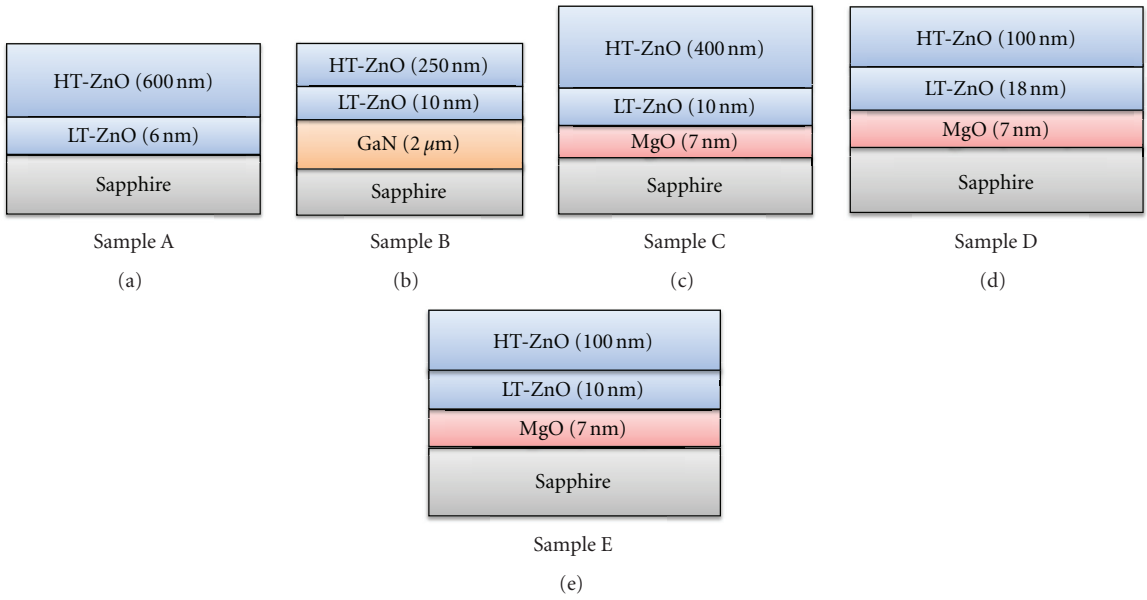

Figure 1: Schematic picture for the layer structures of (a) Sample A, (b) Sample B, (c) Sample C, (d) Sample D, and (e) Sample E used in this work.

Table 1: The growth parameters of ZnO thin film samples.

sample	HT-ZnO growth temperature (°C)	HT-ZnO growth conditions	HT-ZnO thickness (nm)	LT-ZnO	Buffer layer
A	600	O_2-rich	600	500°C 6 nm	N/A
B	600	O_2-rich	250	300°C 10 nm	1000°C 2 μm GaN
C	600	O_2-rich	400	300°C 10 nm	550°C 7 nm MgO
D	600	O_2-rich	100	300°C 18 nm	550°C 7 nm MgO
E	600	$Zn : O_2 = 1 : 1$	100	300°C 10 nm	550°C 7 nm MgO

the MgO buffer can effectively suppress the stretching of threading dislocations to the c-axis of the ZnO layer. The highest degree of crystallinity was achieved for ZnO thin films grown on 7 nm thick MgO buffer layers, which is a fivefold improvement over the 2 μm thick GaN buffer layer.

Table 2 shows the material parameters of ZnO thin film samples obtained from XRD measurement. The grain size of each sample was calculated using the Sherrer equation [22–25]: $D = 0.94\lambda/\beta\cos\theta$. Here D, λ, β, and θ are the grain size, beam wavelength (0.15405 nm), FWHM, and diffraction angle of the XRD measurement, respectively. In Table 2, the lattice parameters a and c were calculated through the Bragg Diffraction equation ($2d\sin\theta = n\lambda$) and the lattice equation of the wurtzite structure (1) [22]:

$$a = d_{hkl}\sqrt{\frac{4}{3}(h^2 + hk + k^2) + l^2\left(\frac{a}{c}\right)^2}, \qquad \frac{a}{c} = \sqrt{\frac{8}{3}}. \tag{1}$$

Here d_{hkl} is the interplanar distance and h, k, l are the Miller Indices. The biaxial stress was calculated by comparing the c-lattice constant to the strain-free lattice parameter ($c_0 = 0.5205$ nm) measured from a ZnO powder sample: $\sigma = -453.6 \times 10^9[(c - c_0)/c_0]$. The strain was calculated by: $\varepsilon = \beta/4\tan\theta$ [22–24, 26].

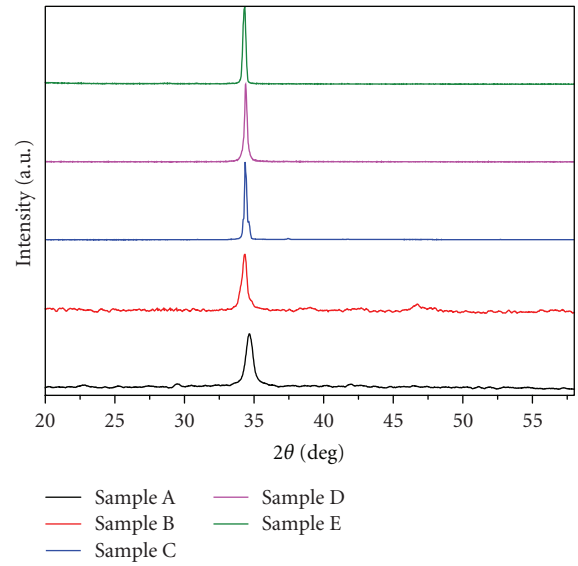

Figure 2: XRD ω-2θ spectra of the Samples A, B, C, D, and E.

Table 2: Peak position, FWHM, grain size, strain, stress, and lattice constants (d) of the samples from XRD measurements and derived lattice parameters (a, c).

Sample	2 theta (degree)	FWHM (acrsec)	Grain size (nm)	Strain (microstrain)	Stress (Gpa)	d (Å)	a (Å)	c (Å)
A	34.68	791.74	37.872	299.624	3.306	2.584	3.164	5.167
B	34.33	242.58	123.493	90.809	−1.171	2.609	3.196	5.218
C	34.37	64.18	466.849	24.057	−0.606	2.606	3.192	5.212
D	34.41	48.66	615.805	18.261	−0.120	2.603	3.188	5.206
E	34.33	98.01	305.715	36.692	−1.145	2.609	3.195	5.218

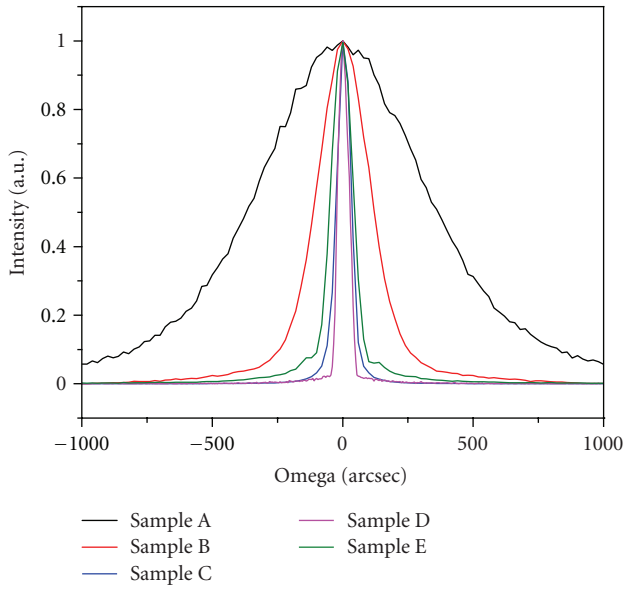

Figure 3: Normalized XRC results of the Samples A, B, C, D, and E.

From these calculations the ZnO layer in Sample A suffered tensile stress of 3.306 GPa and 299.624 microstrain. The high tensile stress caused cracking during the ZnO thin film growth. In Sample B, the ZnO layer suffered compressive stress of −1.171 GPa and 90.809 microstrain. The change from tensile stress to compressive stress using GaN as a buffer layer can solve the problem of the film cracking.

Using MgO as a buffer layer (Samples C, D, and E) resulted in an increased strain release in the ZnO thin film growth. In sample D, the minimum compressive stress (−0.120 GPa) and strain (18.261 microstrain) were observed and were found to be close to the stress-free condition. These results imply that threading dislocations were effectively confined in the ZnO/MgO interface due to the cubic structure of MgO during the ZnO thin film growth [20, 21]. Sample D exhibited the highest crystalline quality ZnO thin film in this study.

4. Deep Level and Edge Band Emission

The PL spectra of the ZnO thin film samples at room temperature (Figure 4(a)) show strong edge band emissions (EBE) with very weak deep level emissions (DLE), which confirms their good crystalline and optical quality. The band-edge emission peaks of the samples are located at 3.312 eV, 3.305 eV, 3.304 eV, 3.298 eV, and 3.317 eV, for Samples A, B, C, D, and E, respectively, while the broad DLE peaks are at about 2.25 eV. The DLE results reveal the presence of defects and oxygen vacancies in the ZnO thin films [25]. In order to compare the optical quality of these samples, the integrated intensity ratio of the EBE to the DLE as a function of temperature for each of the samples is shown in Figure 4(b). The integrated intensity of EBE and DLE ranges from 2.918 eV to 3.758 eV and 1.771 eV to 2.756 eV, respectively, corresponding to the shaded areas in Figure 4(a). The EBE/DLE values decrease rapidly with increasing temperature up to some specific temperature for each of the samples. These specific temperatures are approximately 45 K, 45 K, 75 K, 90 K, and 75 K for Samples A, B, C, D, and E, respectively. Above these specific temperatures, no rapid decrease in EBE/DLE values is observed. The specific temperature represents the critical temperature below which radiative recombination dominates and above which nonradiative recombination dominates. For Sample A the low EBE/DLE values in all temperature ranges represent a higher density of threading dislocations, more stress, and higher defect density in the ZnO thin film, corresponding to the lower optical quality of the sample. The EBE/DLE values increase significantly in the samples with GaN or MgO buffer layers. These results confirm the improvement of ZnO thin film crystallinity from using GaN and MgO buffer layers. When comparing Sample E to Samples C and D, the apparently lower optical quality of Sample E originates from the stoichiometric growth condition ($Zn : O_2 = 1 : 1$). This growth condition induces more oxygen vacancies in the ZnO layer leading to a higher DLE intensity. This order of DLE intensity for the samples is the same for the entire temperature range.

In order to check the consistency between the optical measurements and structural measurements, the integrated intensity ratio of the EBE to the DLE and the inverse FWHM of the XRC of each samples are shown in Figure 5. The maximum EBE/DLE means the EBE/DLE value of sample at 10 K. Higher EBE/DLE ratios and higher values for $FWHM^{-1}$ from XRC measurements represent improved optical and material qualities of the samples. Samples C, D, and E, with MgO buffer layers, show an enhancement of their crystalline and optical qualities. Sample B with a GaN buffer layer exhibits inferior results. Sample A without any buffer layer had the worst quality.

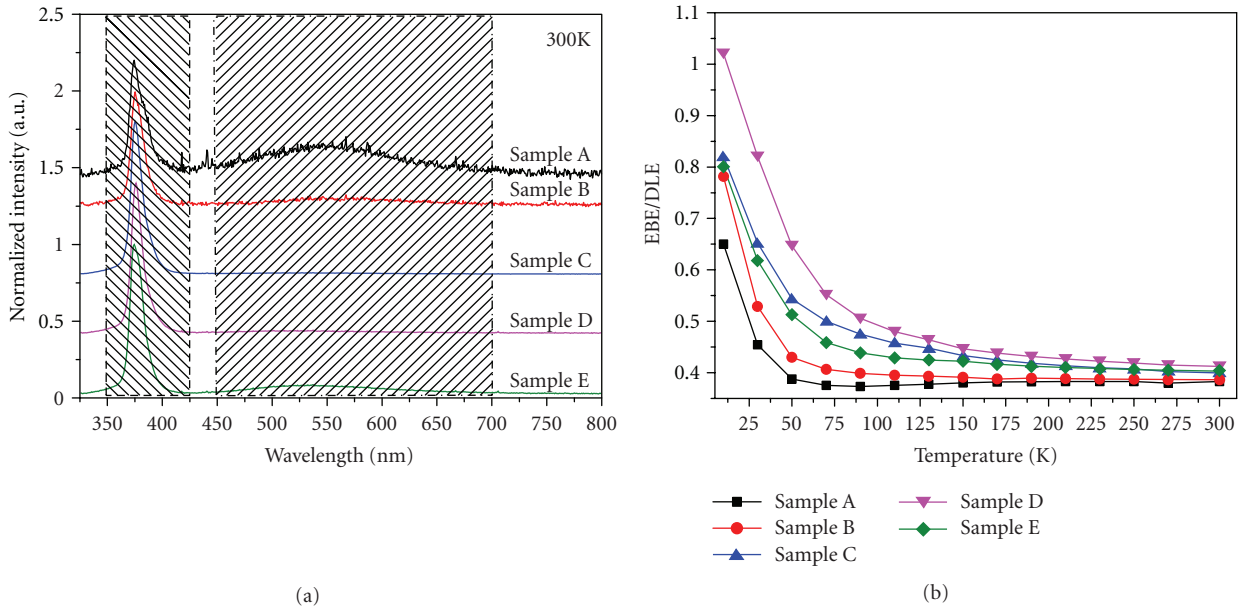

Figure 4: (a) Photoluminescence and deep level emission spectra of the Samples A, B, C, D, and E at room temperature, (b) the integrated intensity ratio of the EBE to the DLE of samples as functions of temperature.

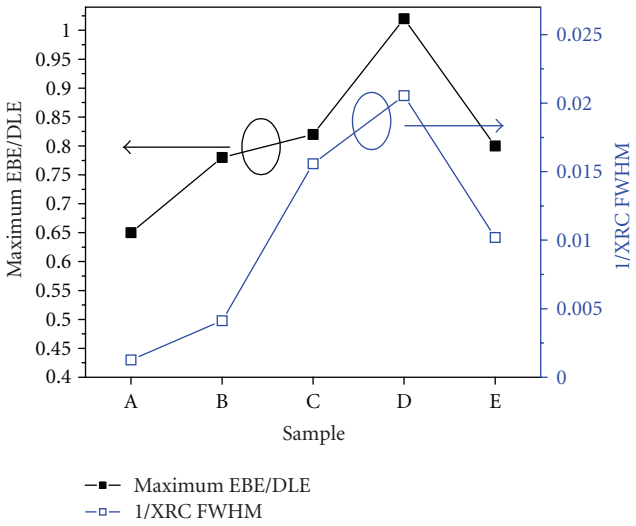

Figure 5: The integrated intensity ratio of the EBE to the DLE and the inverse FWHM of XRC of Samples A, B, C, D, and E.

5. SEM and AFM Images

Figures 6(a) and 6(b) show SEM and AFM images of Samples A and D. In the SEM image of Sample A (Figure 6(a)), surface pits can be seen. The rougher surface of Sample A compared to Sample D originates from the larger lattice mismatch in the ZnO/sapphire interface. The large tensile stress in Sample A is induced by this increased lattice mismatch. AFM measurement reveals a larger root mean square (RMS) roughness of about 6.982 nm without a buffer layer. For the MgO buffer layer in sample D, the RMS roughness is about 2.875 nm. The decrease in RMS roughness by 58.8% is attributed to the change from tensile stress to compressive stress when using the MgO buffer layer compared to no buffer layer. These results indicate that the growth of ZnO thin films on buffer layers, especially MgO, results in better crystallinity of samples, thus improved optical characteristics.

In summary, by including a buffer layer in the growth of ZnO thin films, the lattice mismatch of the film surface to the sapphire substrate surface was decreased significantly. Including a GaN buffer layer in Sample B resulted in higher optical and structural quality than Sample A. The comparison between ZnO growth on the GaN and the MgO buffer layers shows that dislocations stretching along the *c*-axis could not be suppressed effectively by a thick GaN buffer layer. Samples C, D, and E were of higher quality than sample B.

For the MgO buffer layer growth, the stoichiometric growth condition induced more oxygen vacancies in the ZnO layer, resulting in lower crystal quality in Sample E compared to Samples C and D. In the two-step temperature variation growth, the optimal LT-ZnO thickness was about 40 nm for Sample D [11], which showed the highest crystallinity in this study. Thus, the LT-ZnO has an important effect in changing the crystal quality of the following HT-ZnO. The LT-ZnO with optimal thickness could cause relatively disordered HT-ZnO growth on the MgO buffer layer resulting in a three-dimensional island morphology, resulting in different defect configurations in the HT-ZnO layer [11]. From the description above, one can see that the order of ZnO thin film crystallinity, from best to worst, is D, C, E, B, and A.

6. Conclusion

In conclusion, the influence of the GaN and MgO buffer layers on the structural, electrical, and optical properties

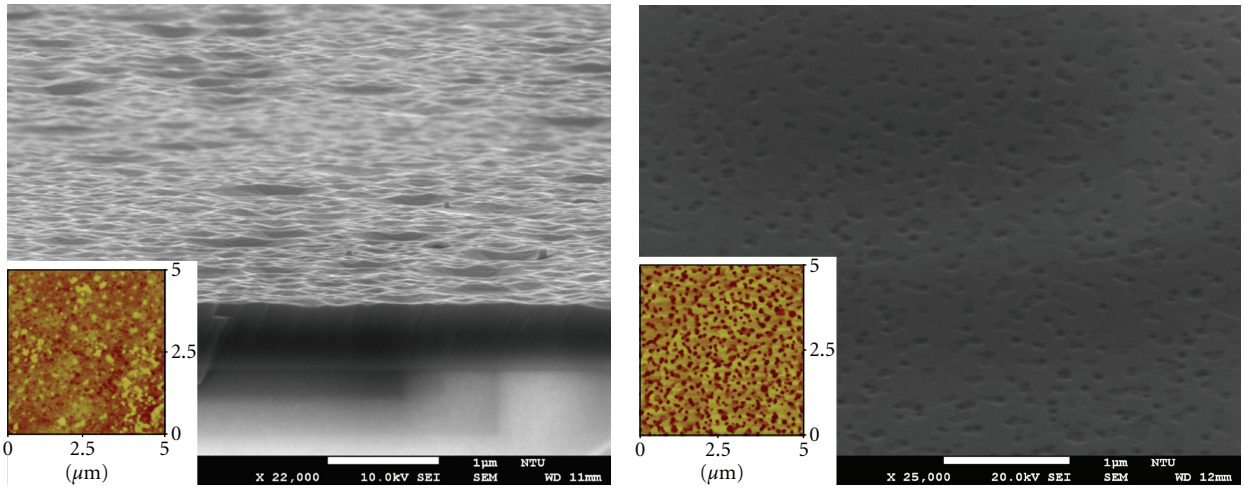

Figure 6: SEM and AFM images of (a) Sample A and (b) Sample D.

of ZnO thin films grown on sapphire substrates by MBE was investigated. The XRD and XRCs investigations revealed that the buffer layer had diminished the strain and changed the stress from tensile to compressive, leading to threading dislocation elimination. The PL revealed a strong edge band emission with a weak deep level emission, suggesting the good crystalline quality of the ZnO thin films on the MgO buffer layer. The increase in the integrated intensity ratio of the EBE to the DLE and the inverse FWHM of XRC with GaN and MgO as buffer layers demonstrated the enhancement of the structural and optical qualities of the ZnO thin films.

Acknowledgments

This research was supported by National Science Council, China, under the Grants of NSC 99-2221-E-002-123-MY3, 100-2622-E-002-008-CC2, 100-2221-E-002-170, 100-2221-E-194-043, by NTU Excellent Research Project (10R80908-B), and by US Air Force Scientific Research Office under the contract of AOARD-11-4114.

References

[1] D. C. Look, "Recent advances in ZnO materials and devices," *Materials Science and Engineering B*, vol. 80, no. 1–3, pp. 383–387, 2001.

[2] D. M. Bagnall, Y. F. Chen, Z. Zhu et al., "Optically pumped lasing of ZnO at room temperature," *Applied Physics Letters*, vol. 70, no. 17, pp. 2230–2232, 1997.

[3] J. H. Lim, C. K. Kong, K. K. Kim, I. K. Park, D. K. Hwang, and S. J. Park, "UV electroluminescence emission from ZnO light-emitting diodes grown by high-temperature radiofrequency sputtering," *Advanced Materials*, vol. 18, no. 20, pp. 2720–2724, 2006.

[4] S. Liang, H. Sheng, Y. Liu, Z. Huo, Y. Lu, and H. Shen, "ZnO Schottky ultraviolet photodetectors," *Journal of Crystal Growth*, vol. 225, no. 2–4, pp. 110–113, 2001.

[5] M. Law, L. E. Greene, J. C. Johnson, R. Saykally, and P. Yang, "Nanowire dye-sensitized solar cells," *Nature Materials*, vol. 4, no. 6, pp. 455–459, 2005.

[6] Q. Wan, Q. H. Li, Y. J. Chen et al., "Fabrication and ethanol sensing characteristics of ZnO nanowire gas sensors," *Applied Physics Letters*, vol. 84, no. 18, pp. 3654–3656, 2004.

[7] Y. Zhang, G. Du, D. Liu et al., "Crystal growth of undoped ZnO films on Si substrates under different sputtering conditions," *Journal of Crystal Growth*, vol. 243, no. 3-4, pp. 439–443, 2002.

[8] S. K. Hong, H. J. Ko, Y. Chen, and T. Yao, "Control of ZnO film polarity," *Journal of Vacuum Science and Technology B*, vol. 20, no. 4, pp. 1656–1663, 2002.

[9] T. Gruber, C. Kirchner, K. Thonke, R. Sauer, and A. Waag, "MOCVD growth of ZnO for optoelectronic applications," *Physica Status Solidi A*, vol. 192, no. 1, pp. 166–170, 2002.

[10] M. Fujita, N. Kawamoto, T. Tatsumi, K. Yamagishi, and Y. Horikoshi, "Molecular beam epitaxial growth of ZnO on Si substrate using ozone as an oxygen source," *Japanese Journal of Applied Physics Part 1*, vol. 42, no. 1, pp. 67–70, 2003.

[11] J. G. Kim, S. K. Han, S. M. Yang et al., "Effects of low temperature ZnO and MgO buffer thicknesses on properties of ZnO films grown on (0001) Al2O3 substrates by plasma-assisted molecular beam epitaxy," *Thin Solid Films*, vol. 519, no. 1, pp. 223–227, 2010.

[12] Y. J. Chen, Y. Y. Shih, C. H. Ho, J. H. Du, and Y. P. Fu, "Effect of temperature on lateral growth of ZnO grains grown by MOCVD," *Ceramics International*, vol. 36, no. 1, pp. 69–73, 2010.

[13] X. Q. Wang, H. P. Sun, and X. Q. Pan, "Effect of GaN interlayer on polarity control of epitaxial ZnO thin films grown by molecular beam epitaxy," *Applied Physics Letters*, vol. 97, no. 15, Article ID 151908, 2010.

[14] B. Pecz, A. El-Shaer, A. Bakin, A. C. Mofor, A. Waag, and J. Stoemenos, "Structural characterization of ZnO films grown by molecular beam epitaxy on sapphire with MgO buffer," *Journal of Applied Physics*, vol. 100, no. 10, Article ID 103506, 2006.

[15] A. A. Ashrafi, A. Ueta, H. Kumano, and I. Suemune, "Role of ZnS buffer layers in growth of zincblende ZnO on GaAs substrates by metalorganic molecular-beam epitaxy," *Journal of Crystal Growth*, vol. 221, no. 1–4, pp. 435–439, 2000.

[16] Z. D. Sha, J. Wang, Z. C. Chen et al., "Initial study on the structure and optical properties of ZnO film on Si(1 1 1) substrate with a SiC buffer layer," *Physica E*, vol. 33, no. 1, pp. 263–267, 2006.

[17] B. M. Ataev, W. V. Lundin, V. Mamedov, A. M. Bagamadova, and E. E. Zavarin, "Low-pressure chemical vapour deposition growth of high-quality ZnO films on epi-GaN/α-Al2O3," *Journal of Physics Condensed Matter*, vol. 13, no. 9, pp. L211–L214, 2001.

[18] J. P. Cui, Y. Duan, X. F. Wang, and Y. P. Zeng, "Strain status in ZnO film on sapphire substrate with a GaN buffer layer grown by metal-source vapor phase epitaxy," *Microelectronics Journal*, vol. 39, no. 12, pp. 1542–1544, 2008.

[19] A. Bakin, J. Kioseoglou, B. Pecz et al., "Misfit reduction by a spinel layer formed during the epitaxial growth of ZnO on sapphire using a MgO buffer layer," *Journal of Crystal Growth*, vol. 308, no. 2, pp. 314–320, 2007.

[20] Y. Chen, H. J. Ko, S. K. Hong, and T. Yao, "Layer-by-layer growth of ZnO epilayer on Al2O3(0001) by using a MgO buffer layer," *Applied Physics Letters*, vol. 76, no. 5, pp. 559–561, 2000.

[21] Y. Chen, S. K. Hong, H. J. Ko et al., "Effects of an extremely thin buffer on heteroepitaxy with large lattice mismatch," *Applied Physics Letters*, vol. 78, no. 21, pp. 3352–3354, 2001.

[22] P. Singh, A. Kumar, Deepak, and D. Kaur, "ZnO nanocrystalline powder synthesized by ultrasonic mist-chemical vapour deposition," *Optical Materials*, vol. 30, no. 8, pp. 1316–1322, 2008.

[23] W. Taeg Lim and C. Hyo Lee, "Highly oriented ZnO thin films deposited on Ru/Si substrates," *Thin Solid Films*, vol. 353, no. 1, pp. 12–15, 1999.

[24] J. Ye, S. Gu, S. Zhu et al., "The growth and annealing of single crystalline ZnO films by low-pressure MOCVD," *Journal of Crystal Growth*, vol. 243, no. 1, pp. 151–156, 2002.

[25] B. H. Kong, D. C. Kim, S. K. Mohanta, and H. K. Cho, "Influence of VI/II ratios on the growth of ZnO thin films on sapphire substrates by low temperature MOCVD," *Thin Solid Films*, vol. 518, no. 11, pp. 2975–2979, 2010.

[26] D. Sahu, B. S. Acharya, and A. K. Panda, "Role of Ag ions on the structural evolution of nano ZnO clusters synthesized through ultrasonication and their optical properties," *Ultrasonics Sonochemistry*, vol. 18, no. 2, pp. 601–607, 2011.